Hindawi Publishing Corporation
Advances in Materials Science and Engineering
Volume 2011, Article ID 485942, 7 pages
doi:10.1155/2011/485942

Research Article

Synthesis and Characterization of High-Entropy Alloy Al_XFeCoNiCuCr by Laser Cladding

Xiaoyang Ye,[1] Mingxing Ma,[1] Wenjin Liu,[1] Lin Li,[1,2] Minlin Zhong,[1] Yuanxun Liu,[1] and Qiwen Wu[1]

[1] *Key Laboratory for Advanced Materials Processing Technology Ministry of Education, Department of Mechanical Engineering, Tsinghua University, Beijing 100084, China*
[2] *Laser Processing Research Centre, School of Mechanical, Aerospace and Civil Engineering, The University of Manchester, Manchester M13 9PL, UK*

Correspondence should be addressed to Mingxing Ma, mmx.thudme@gmail.com

Received 31 August 2010; Accepted 22 December 2010

Academic Editor: J. Dutta Majumdar

High-entropy alloys have been recently found to have novel microstructures and unique properties. In this study, a novel Al_XFeCoNiCuCr high-entropy alloy was prepared by laser cladding. The microstructure, chemical composition, and constituent phases of the synthesized alloy were characterized by SEM, EDS, XRD, and TEM, respectively. High-temperature hardness was also evaluated. Experimental results demonstrate that the Al_XFeCoNiCuCr clad layer is composed of only BCC and FCC phases. The clad layers exhibit higher hardness at higher Al atomic content. The AlFeCoNiCuCr clad layer exhibits increased hardness at temperature between 400–700°C.

1. Introduction

The component of an alloy system is usually based on one principle element and some additional elements for a superior performance. It makes use of the edge component region in the phase diagrams. The traditional view holds that although it is helpful to add a small amount of alloying elements for better performance, a large quality of the additional alloying elements should be avoided. In some of the common traditional alloys such as aluminum alloy and nickel or titanium alloys, the main elements usually take up more than 50% atomic content.

The widely used ferroalloys suffer a fall of hardness when they are tempered at 350–550°C, which limits the possible applications in high-temperature environments [1]. The high-temperature precipitate strengthened nickel-base super alloys, which are widely applied in the aviation industry, also suffer from the same problem, although to a lesser degree. The multiprinciple bulk metallic glasses crystallize at 400–600°C, which also limits the application in high temperature [2]. Poor performance in high temperature restricts the application of tradition alloys.

As discussed above, the traditional way of designing an alloy restricts the development of alloy systems for high-temperature and extreme-loading applications. The introduction of the high-entropy alloys (HEA) concept by Yeh et al. [3] broke up the traditional rule that the main elements take up more than 50% atomic content. HEA means that alloys are composed of multielements and each takes up a relatively high but less than 35% of atomic content. The properties of this innovative alloy are decided by the combined action of multielements. Previous research demonstrates that the high-entropy alloy tends to form simple crystallization phase disorderly, even nanophase or amorphous phase. At the same time, by controlling the composition, it is possible to achieve high-hardness and high-abrasion performance at high temperatures [4].

Vacuum arc remelting [5–9] for bulk cast ingot is the primary method to synthesize HEAs. Surface coating is also possible. Varalakshmi et al. [10] synthesized the AlFeTiCrZnCu by mechanical alloying. However, these methods can hardly be directly applied for the surface modification. By ball milling followed by cladding on the surface, the alloy powder can be used for surface modification indirectly.

The bulk-processing route can be costly and is limited to the production of relatively small components. However, in many situations, only the contact surface properties are important in determining performance of the component in practical applications. Therefore, the use of a coating has several attractive advantages.

In this paper, a novel method to fabricate the HEA coatings by laser cladding is reported. Due to rapid heating and cooling in the laser cladding process, the cooling rate of laser cladding can reach 10^3–10^6 K/s. More importantly, laser cladding has the capability of achieving a controllable dilution ratio, metallurgical bonding between the coating and the substrate, small thermal deformation, and nonequilibrium reaction. Considering HEA's tendency to form simple structures and nanocrystallines, fabricating HEA by laser cladding is of great significance and potential for extensive use. Until now, this new method has not been reported elsewhere. The objective of the investigation is to ascertain the feasibility of fabricating HEA by laser cladding and achieve alloy coatings with good combination properties, with an emphasis on high-temperature hardness.

2. Experimental Procedures

Al, Co, Cr, Ni, Cu, and Fe powders of high purity are prepared and well mixed as the raw material. Before the above powder material is preplaced on an AISI 1045 steel substrate, the mixed powders are added with ethanol and mixed uniformly. The thickness of the precoated powder layers was restricted to approximately 1.4 mm. When the thickness is as large as the 1.6 mm, the number and length of the cracks will increase sharply. However, when the thickness is as small as 1.0 mm, it is difficult to obtain the approximate dilution rate by controlling the laser parameters. With a PRC-3000 CO_2 laser equipment, in the argon environment, the HEA was synthesized on the surface of AISI 1045 steel. The performance of the cladding coatings are controlled by the laser power and scanning speed, and the spot diameter is fixed to 3 mm. Several different values of laser power were used for laser cladding: 1200 W to 2000 W. The scanning speed is among 2 mm/s–12 mm/s.

It has been reported that Al has a significant influence on the structure and properties [11]. In order to evaluate the influence of Al content in Al_XFeCoNiCuCr coatings by laser cladding, the X factor was set as another variable quantity and the experiments were divided into 5 groups: $X = 1$, 1.3, 1.5, 1.8, and 2.0. All the elements except Al are equiatomic. After the laser cladding, the specimens were sectioned perpendicular to the scanning track with a wire-EDM machine. The specimens were analyzed by a D8 Advance X-ray Diffraction analysis system (XRD). The chemical composition of the cladding was determined by an Oxford INCA X-sight 7573 Energy Dispersive X-ray (EDX) microanalysis system equipped with JSM-6460LV Scanning Electron Microscope (SEM). The crystal structure of the cladding layers were analyzed by JEOL-JEM-2010 transmission electron microscope (TEM). The microhardness was measured with an HX-200 Vickers Hardness Tester and the high-temperature microhardness was measured at 200–800°C with an AKASHI AVK-A High-Temperature Micro Hardness Tester.

3. Results and Discussion

3.1. Synthesis of High-Entropy Alloys. By optimizing the laser parameters, porosity-free alloy coatings were synthesized by laser cladding. The optimal ranges of laser powers and scanning speeds for better dilution rate are among 1400–1800 W and 8–12 mm/s, respectively. Figure 1 shows the macroscopic appearance of coatings. Cracks were avoided when the X values are under 1.5. The coating shows no visible defects in macroscopic views. With the further addition of Al element and the X factor reaching 1.8, some cracks in small number were observed on the coatings. When X reaches 2.0, the number of cracks increases sharply. The sharply elongated cracks run through the cladding layers. The existence of cracks would lead to adverse impacts to the performance of the cladding layers.

3.2. The Microstructure and Compositional Characteristics of Al_XFeCoNiCuCr. The SEM pictures in Figure 2 show the typical central area of the Al_XFeCoNiCuCr structures. The typical structures are composed of both dendritic (DR) and interdendritic (ID) areas. Table 1 shows the atomic composition of both DR and ID.

From Table 1, it can be seen that the actual composition percentage of Fe element is much larger than the nominal one. The possible reason is that some of the Fe element of AISI 1045 steel base dilutes the clad, which results in the deviation from the nominal percentage. Experimental results show that the deviation of Fe elements grew bigger with higher laser power and lower scanning speed. For instance, at 1800 W and 4 mm/s, the atomic percentage of Fe can reach as high as 50%.

The deviation from nominal composition of Al element, indicates that there is a possibility of vaporization of Al during laser cladding. Another possible reason is the selective corrosion of aqua regia. If the corrosion resistance of the Al-enriched phase is poorer than others, this phase would be selectively corroded into interdendritic structure. This situation could also result in the deviation of Al composition.

It was reported that the Cu element could be enriched in the interdendritic structure [10, 11]. The atomic percentage of Cu element would be up to more than 50%. However, laser cladding synthesized Al_XFeCoNiCuCr alloys appear little dendrite segregation between the ID and DR structures. Although the dendrite segregation does occur between the ID and DR, it is not as severe as in casting alloys. The high cooling rate character of laser cladding may explain this phenomenon. In normal situation, with a lower cooling rate, the segregation is more significant. When the cooling rate rises to a certain level, the interdendritic segregation diminishes. This is when the cooling speed reaches a threshold level, then the diffusion process is inhibited in both the solid and liquid phases. Under this condition, the alloy comes into a situation of diffusionless crystallization, similar

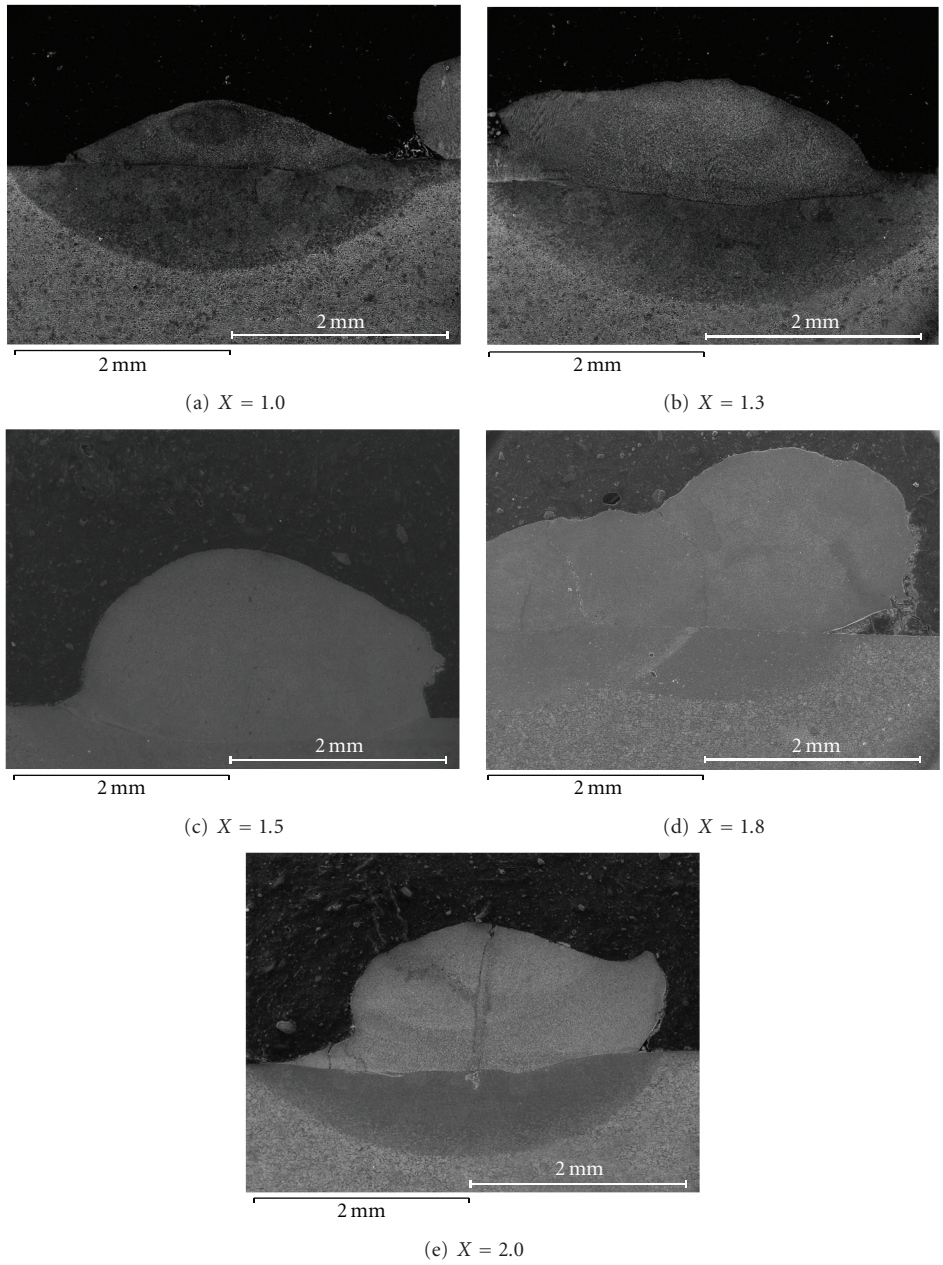

(a) $X = 1.0$ (b) $X = 1.3$

(c) $X = 1.5$ (d) $X = 1.8$

(e) $X = 2.0$

Figure 1: Macroscopic SEM figures of Al_XFeCoNiCuCr High-entropy alloys under different X values at (a) $X = 1$, (b) $X = 1.3$, (c) $X = 1.5$, (d) $X = 1.8$, and (e) $X = 2.0$.

to the solidification process of a pure metal. Hence, the interdendritic segregation in the HEA synthesized by laser cladding should be smaller than that synthesized by casting. Interdendritic segregation usually causes adverse impacts on the alloy's performance, especially on the plasticity and toughness. From the above results, it is expected that alloys fabricated by laser cladding should have better performance than casting ones.

3.3. The Phase Characteristics and the Influence of the Al Contents. The work shows that the atomic content of the Al element has a great influence on the phase composition of HEA Al_XFeCoNiCuCr. Experimental samples with an X factor at 1.0, 1.3, 1.5, 1.8, and 2.0 were characterized using XRD and TEM to understand the phase transitions.

3.3.1. X-Ray Diffraction Analysis. Figure 3 shows the X-ray Diffraction patterns of Al_XFeCoNiCuCr under different X values. The diffraction peaks show that the complex intermetallic compounds are merged into simple phases. Al_XFeCoNiCuCr synthesized by vacuum arc remelting and mechanical alloying are both composed of simple phases [11, 12].

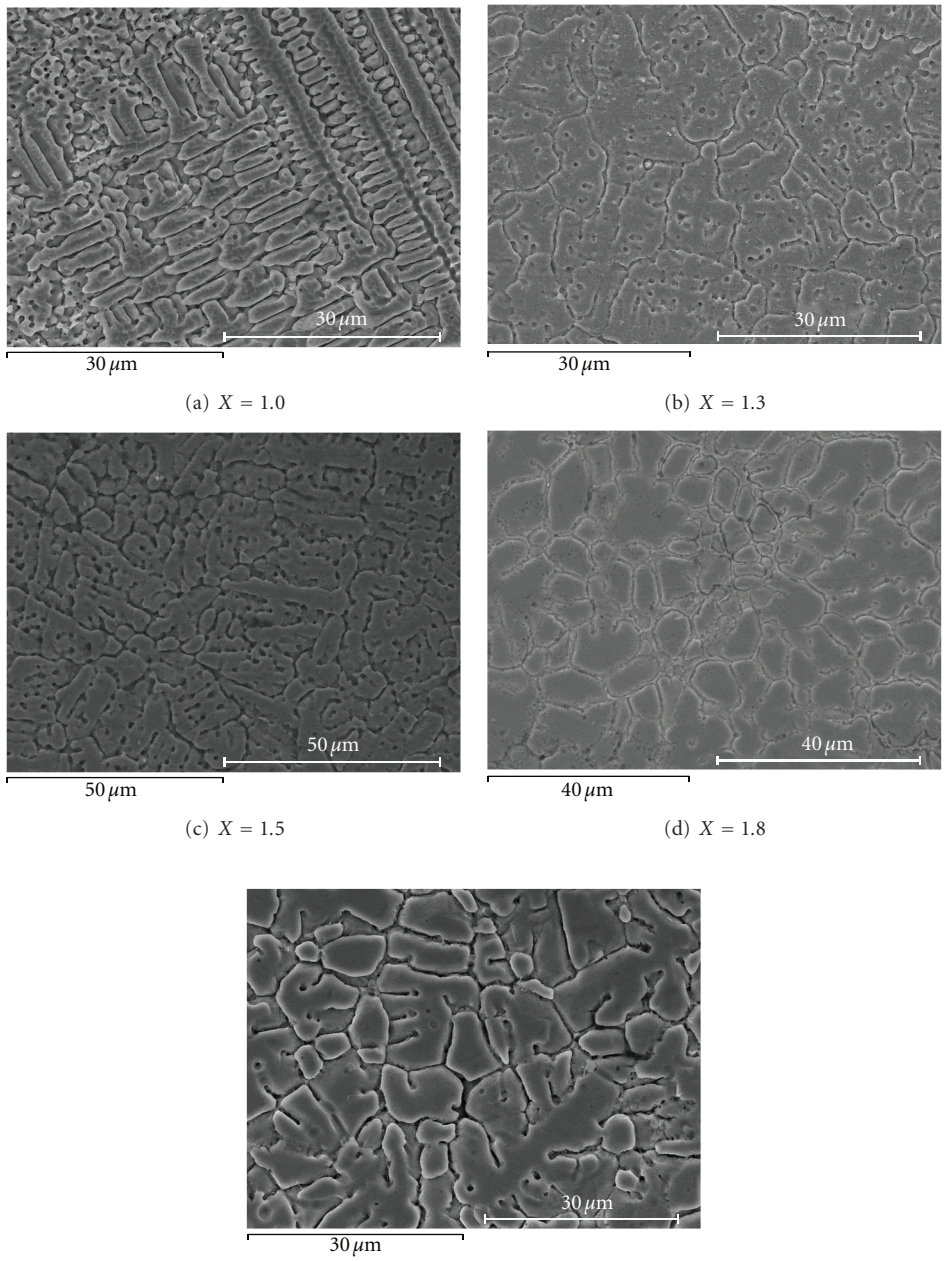

FIGURE 2: Typical microstructure of Al_XFeCoNiCuCr clad layer, etching in aqua regia for a few minutes: (a) $X = 1.0$, (b) $X = 1.3$, (c) $X = 1.5$, (d) $X = 1.8$, and (e) $X = 2.0$.

The analysis shows that Al_XFeCoNiCuCr synthesized by laser cladding shares the same phase composition with the alloys fabricated by traditional methods. According to Figure 4, the addition of Al content does not change the number of phases. However, the relative intensity of the FCC diffraction peaks decrease and the BCC peaks increase. It can be inferred that there exists the transition from FCC phase to the BCC phase, accompanied with the addition of Al element. As Al obtains relatively bigger atomic radius, the addition of Al aggravates the lattice distortion. This phenomenon was also observed in previous research [12].

3.3.2. The Transmission Electron Microscope Analysis of AlFeCoNiCuCr. The nanocrystalline nature of the HEA AlFeCoNiCuCr has been confirmed from the TEM bright field image and the corresponding selected area diffraction (SAD) pattern shown in Figure 5.

We can learn that the alloy is composed of two distinct phases: Phase One appears as white spots and Phase Two as a black base. In (a), the microstructure investigation shows the granular Phase One is dispersed in the base of Phase Two. The result also proves the nonentity of the complex intermetallic compounds in the HEA prepared by laser

Table 1: The atomic composition and distribution in different X values.

Alloy	Zone	at%					
		Al	Cr	Fe	Co	Ni	Cu
$Al_{1.0}FeCoNiCuCr$	Nominal	16.66	16.66	16.66	16.66	16.66	16.66
	Actual	5.95	11.34	40.16	11.83	12.82	17.94
	DR	5.64	12.42	42.36	12.94	11.70	14.94
	ID	6.91	11.61	44.18	14.18	10.58	12.53
$Al_{1.3}FeCoNiCuCr$	Nominal	20.63	15.87	15.87	15.87	15.87	15.87
	Actual	14.84	16.28	23.93	15.68	15.71	13.46
	DR	15.29	17.47	25.63	17.71	14.20	9.71
	ID	16.46	16.97	21.67	14.22	16.16	14.53
$Al_{1.5}FeCoNiCuCr$	Nominal	23.08	15.38	15.38	15.38	15.38	15.38
	Actual	14.30	17.84	23.61	15.75	15.12	13.38
	DR	14.78	20.69	27.70	16.56	11.34	8.93
	ID	10.99	15.85	25.96	15.40	15.79	16.01
$Al_{1.8}FeCoNiCuCr$	Nominal	26.47	14.71	14.71	14.71	14.71	14.71
	Actual	20.99	14.92	16.36	16.28	14.65	16.80
	DR	19.10	15.66	22.73	17.89	14.53	10.10
	ID	20.41	14.73	18.57	13.81	16.66	15.82
$Al_{2.0}FeCoNiCuCr$	Nominal	28.57	14.29	14.29	14.29	14.29	14.29
	Actual	17.06	13.68	21.52	16.28	15.12	16.34
	DR	17.89	12.68	27.62	13.57	14.92	13.32
	ID	5.63	13.58	25.88	15.51	20.19	19.21

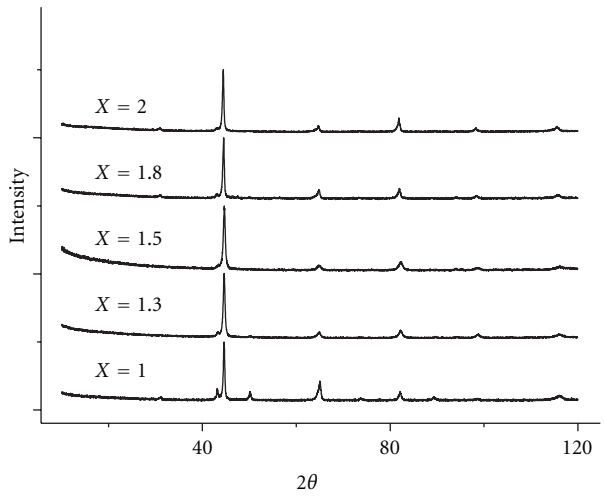

Figure 3: The X-ray Diffraction patterns.

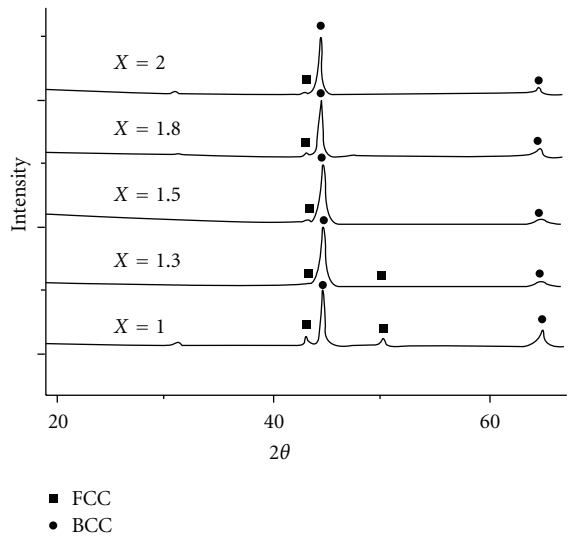

Figure 4: The detailed main diffraction peak of XRD.

cladding. The Phase One is nanostructure, and the average diameter was between several nanometers to about 100 nm.

3.4. The Cladding Layer Microhardness Distribution of $Al_XFeCoNiCuCr$. For the cladding layers, the microhardness is a key performance index. It is also reported that the content of Al elements has a great influence on the hardness [12]. The microhardness distribution for different X values and the average hardness are shown, respectively, in Figure 6 and Table 2.

Table 2: The microhardness in different X values ($HV_{0.2}$).

Al composition	$X = 1.0$	$X = 1.3$	$X = 1.5$	$X = 1.8$	$X = 2.0$
Average $HV_{0.2}$	390	540	640	660	687
Average HRC	40	52	58	58	60

The microhardness values for different X factors differ considerably. With the increase of X, the average microhardness across a section of the cladding layers (0–10 mm

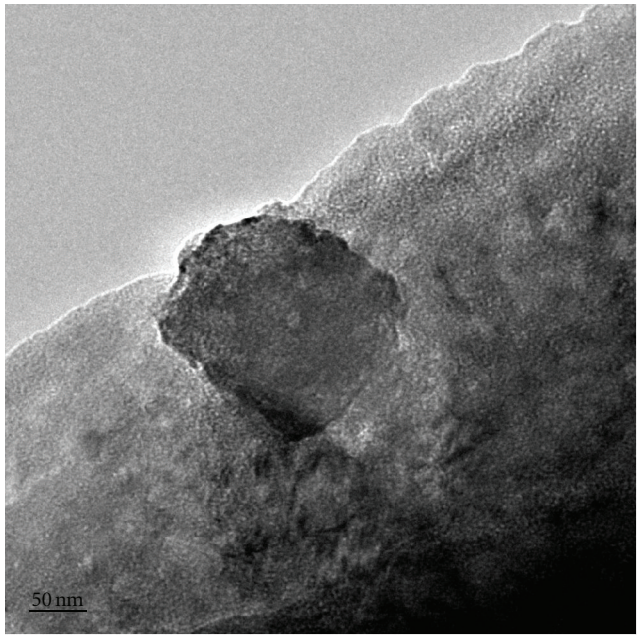

(a)

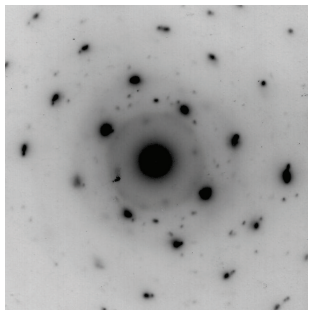

(b)

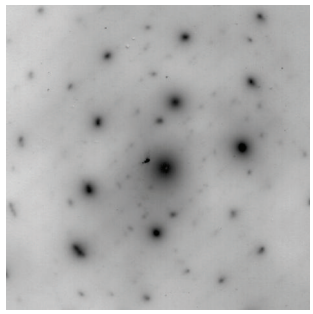

(c)

Figure 5: The TEM image and SAD patterns. (a) Bright field image; (b) SAD pattern of [001] zone axis; (c) SAD pattern of BCC [012] zone axis.

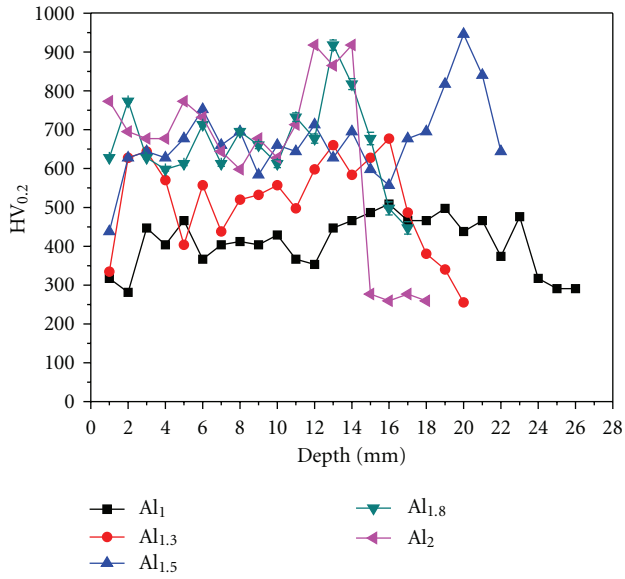

Figure 6: The microhardness distribution in different X values (X = 1, 1.3, 1.5, 1.8, and 2.0).

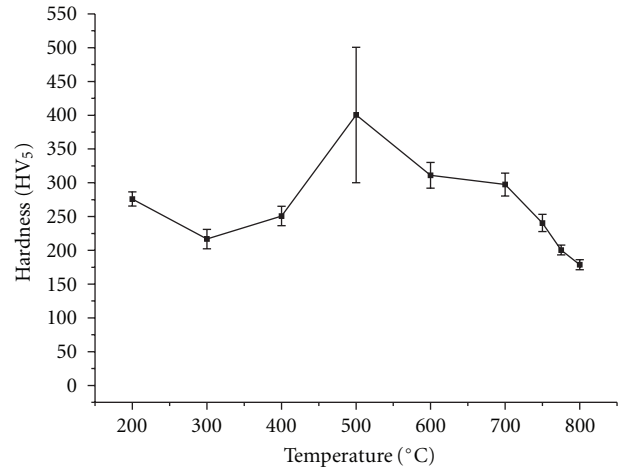

Figure 7: The high-temperature microhardness distribution.

in length) presents an increasing trend with the increases in the X factor. When the X value increases from 1 to 2, the average microhardness increases from 390 to 687 $HV_{0.2}$. The content of Al significantly influences the microhardness. This result is in agreement with the reported research [11]. This phenomenon can be explained in the transition of lattice structure. As discussed above, the addition of Al promotes the transition from FCC to BCC structure. With the further addition, the BCC become the elementary phase, which results in a significant change of the microstructure. As the BCC structure is considered to obtain higher hardness than FCC [12], the microhardness would expect a sharp increase after this transition. In another aspect, for the bigger atomic ratio of Al, the atoms serve as a function of solution strengthening and aggravate the lattice distortion. Compared with the casting alloys, HEA synthesized by laser cladding obtains higher microhardness as a result of more rapid cooling which leads to finer microstructures.

From Table 2, it can be inferred that the increase of microhardness is sharp when the X increases from 1.0 to 1.5. With further addition of Al, the increasing rate of microhardness slows down because the initial addition of Al greatly change the phase structure and this effect diminishes gradually during further addition.

However, the addition of Al also results in the increasing of cracks. It is possible to seek a balanced X values in which lie the higher average microhardness and less defects. This optimal X lies between 1.5 and 1.8.

3.5. High-Temperature Microhardness. Previous research focuses on the microhardness change after tempering in different temperatures instead of the hardness in high-temperature situations. If HEA could remain a high hardness in high temperature, the possible applications could be

greatly increased. In this paper, we choose AlFeCoNiCuCr for the high-temperature hardness test. Figure 7 shows the microhardness of AlFeCoNiCuCr at different temperatures. Firstly, when the alloy was heated, there was an obvious fall of hardness. Most alloys would suffer from a fall of hardness when heated.

However, more importantly, as the temperature further increases to between 400°C and 500°C, the hardness has a sharp increase. Higher hardness than that at room temperature is shown for temperatures between 400°C and 700°C. This phenomenon shows that the AlFeCoNiCuCr alloy shares the same property as high-speed steel which also has an increasing hardness trend in certain temperature ranges. High-speed steel contains elements such as W, Mo, Cr, Co, and V, which can result in the carbide precipitation when tempering. Precipitation harden effect serve as harden mechanism. When it comes to HEA this phenomenon can be explained as the multialloying elements form intermetallic compounds of high thermostability and microhardness, which results in higher high temperature hardness at temperatures between 400–700°C. This property undoubtedly enhances the possible application in high-temperature situations. However, the hardness falls sharply at 600–800°C and finally reaches $HV_{5.0}150$. This is far from the average hardness in room temperature. Both HEA and high-speed tool steel suffer from a hardness fall above about 600°C.

4. Conclusion

High-entropy alloys Al_XFeCoNiCuCr has been successfully in situ synthesized by laser cladding, and they are proved to obtain nanostructure. The following characteristics of the alloy have been found.

(1) Optimal laser parameters of synthesizing Al_XFeCoNiCuCr for suitable dilution ratio are 1400–1800 W and 8–12 mm/s.

(2) The HEAs prepared by laser cladding have shown homogeneity in composition and have a crystallite size of about 10 nm.

(3) Nanostructure with BCC and FCC crystal structure have been observed in all the compositions. The addition of Al element promotes the transition of FCC to BCC structure.

(4) The composition of Al element is a key factor influencing the microhardness and forming of HEA. The alloy combines the relatively balanced forming and microhardness at the composition region where $X = 1.5$ to $X = 1.8$.

(5) The nanocrystalline high entropy alloy is stable even at 400–700°C and has a higher microhardness than that at room temperature. The hardness presents a sharp increase between 400°C and 500°C. However, reduced hardness at temperatures above 700°C was also observed.

Acknowledgments

The authors would like to thank Liang Lv for technical assistance in TEM experiments and Yu Gu and Changsheng Dong for processing the figures. X. Ye would like to acknowledge the financial support by Professor Wenjin Liu and Dr. Mingxing Ma.

References

[1] C. W. Yao, J. Huang, P. L. Zhang, YI. X. Wu, and B. S. Xu, "Tempering softening of overlapping zones during multi-track laser quenching for carbon steel and alloy steel," *Transactions of Materials and Heat Treatment*, vol. 30, no. 5, pp. 131–135, 2009.

[2] K. B. Kim, P. J. Warren, and B. Cantor, "Structural relaxation and glass transition behavior of novel $(Ti_{33}Zr_{33}Hf_{33})_{50}(Ni_{50}Cu_{50})_{40}Al_{10}$ alloy developed by equiatomic substitution," *Journal of Non-Crystalline Solids*, vol. 353, no. 32-40, pp. 3338–3341, 2007.

[3] J. W. Yeh, S. K. Chen, SU. J. Lin et al., "Nanostructured high-entropy alloys with multiple principal elements: novel alloy design concepts and outcomes," *Advanced Engineering Materials*, vol. 6, no. 5, pp. 299–303, 2004.

[4] A. Inoue, "Bulk amorphous alloys with soft and hard magnetic properties," *Materials Science and Engineering A*, vol. 226-228, pp. 357–363, 1997.

[5] F. J. Wang and Y. Zhang, "Effect of Co addition on crystal structure and mechanical properties of Ti0.5CrFeNiAlCo high entropy alloy," *Materials Science and Engineering A*, vol. 496, no. 1-2, pp. 214–216, 2008.

[6] Y. Zhang, Y. J. Zhou, J. P. Lin, G. L. Chen, and P. K. Liaw, "Solid-solution phase formation rules for multi-component alloys," *Advanced Engineering Materials*, vol. 10, no. 6, pp. 534–538, 2008.

[7] C. J. Tong, M. R. Chen, S. K. Chen et al., "Mechanical performance of the Al_XCoCrCuFeNi high-entropy alloy system with multiprincipal elements," *Metallurgical and Materials Transactions A*, vol. 36, no. 5, pp. 1263–1271, 2005.

[8] C. J. Tong, Y. L. Chen, S. K. Chen et al., "Microstructure characterization of Al_XCoCrCuFeNi high-entropy alloy system with multiprincipal elements," *Metallurgical and Materials Transactions A*, vol. 36, no. 4, pp. 881–893, 2005.

[9] B. S. Li, Y. P. Wang, M. X. Ren, C. Yang, and H. Z. Fu, "Effects of Mn, Ti and V on the microstructure and properties of AlCrFeCoNiCu high entropy alloy," *Materials Science and Engineering A*, vol. 498, no. 1-2, pp. 482–486, 2008.

[10] S. Varalakshmi, M. Kamaraj, and B. S. Murty, "Synthesis and characterization of nanocrystalline AlFeTiCrZnCu high entropy solid solution by mechanical alloying," *Journal of Alloys and Compounds*, vol. 460, no. 1-2, pp. 253–257, 2008.

[11] L. Yuan and C. Min, "Microstructure and solidification mode of AlTiFeNiCuCrx high-entropy alloy with multi-principal elements," *Special Casting & Nonferrous Alloys*, no. S1, 2008.

[12] Y. Liu, M. Chen, Y. Li, and X. Chen, "Microstructure and mechanical performance of Al_X CoCrCuFeNi high-entropy alloys," *Rare Metal Materials and Engineering*, vol. 38, no. 9, pp. 1602–1607, 2009.